Investigation of the Optical Properties of $Pb_{1-x}Cd_xTe$ Films using Spectroscopic Ellipsometry

Samuel Kovach[1], Oleg Maksimov[2], Pijush Bhattacharya[2], and Frank Peiris[1]*

*corresponding author e-mail: peirisf@kenyon.edu.edu

[1]Department of Physics, Kenyon College, Gambier, Ohio 43022, USA.

[2]Radiation Monitoring Devices, Inc., Watertown, Massachusetts 02472, USA.

Abstract

Using spectroscopic ellipsometry, we studied the optical properties of four $Pb_{1-x}Cd_xTe$ ($0 \leq x \leq 0.20$) films. The $Pb_{1-x}Cd_xTe$ films, deposited on silicon substrates using an electron-beam deposition technique, show a rock-salt structure, with their lattice constants decreasing as a function of Cd concentration. Ellipsometry measurements, which covered a wide spectral range between 0.1 eV to 4.1 eV, determined the index of refraction and the extinction coefficient of the films. As the Cd concentration increases from 0% to 20% in the $Pb_{1-x}Cd_xTe$ films, the index of refraction decreases by ~10%, across the entire energy range. Similarly, there seems to be a decrease in the extinction coefficient with the increase of Cd concentration. An oscillator model, depicting the optical functions of each $Pb_{1-x}Cd_xTe$ film, allowed us to obtain the band gap of each film which blue-shifts as the Cd concentration is increased. Besides the fundamental band gap,

we recovered the higher-order electronic transitions that occur in the Brillouin zone of the $Pb_{1-x}Cd_xTe$ lattice.

Keywords: Spectroscopic ellipsometry; Lead cadmium telluride; Vertical Bridgman; Critical Points

Introduction

Due to their electrical, optical and thermal properties, $Pb_{1-x}Cd_xTe$ alloys have attracted much attention from the research community in the past decade. In particular, the PbTe binary semiconductor, which exhibits a narrow fundamental band gap, has been combined with CdTe to produce mid-infrared optoelectronic devices, such as light-emitting diodes, lasers and detectors.[1–3] Besides optoelectronic applications, PbTe has been explored for its thermal properties [4–6] as well as for its electrical properties, such as forming a two-dimensional electron gas with high mobility.[7] In addition, PbTe-based heterostructures are known to exhibit topological insulator properties.[8] All of these applications can benefit from having alloys of $Pb_{1-x}Cd_xTe$, where their optical, thermal and electrical properties can be tuned to suite a specific application.[9] For instance, ideally, the band gap of $Pb_{1-x}Cd_xTe$ can be tuned over 1 eV, spanning from the band gap of PbTe (320 meV)[10] to the band gap of CdTe (1.53 eV)[11], which will be advantageous in producing optical devices using this alloy system. Alloys of PbTe and CdTe can be used to produce mid-infrared resonant cavity enhanced detectors and vertical external cavity surface emitting lasers, similar to the methods involved in using $Pb_{1-x}Sr_xTe$ alloys for such applications.[2] Additionally, PbTe and $Pb_{1-x}Cd_xTe$ films also can be used to fabricate two-color infrared detectors, operating simultaneously in mid-infrared (PbTe absorber) and near-infrared ($Pb_{1-x}Cd_xTe$ absorber) regions.

Unfortunately, due to the low solubility of both PbTe and CdTe, and the fact that PbTe crystallizes in the rock-salt structure while the CdTe crystallizes in the zinc-blende structure, the realization of $Pb_{1-x}Cd_xTe$ alloys, spanning the entire range, has been challenging. In general, the most common method used to fabricate $Pb_{1-x}Cd_xTe$ has been the Bridgman crystal growth technique.[9] In order to mitigate phase separation issues, most studies have restricted the $Pb_{1-x}Cd_xTe$ alloys to below 20% of Cd.

Spectroscopic ellipsometry (SE) is a non-destructive optical method that can be employed to determine the optical constants [i.e., index of refraction (n) and the extinction coefficient (k)] and the thickness of films in a structure. [12] In contrast to experimental methods such as transmission or reflectivity, SE does not require one to perform Kramers–Kronig transformation. Additionally, the n and k obtained from SE can be further analyzed to obtain the fundamental band gap as well as the higher order electronic transitions, providing insights into the band structure of the material. [13,14] Since SE is an inverse-problem, the experimental data must be fit to an optical model in order to obtain the optical and the geometrical parameters of a sample.

While there are few reported studies on the density functional theory-calculations of the band structure of PbTe[15,16] and $Pb_{1-x}Cd_xTe$[17], there is a scarcity of experimentally determined optical data for these compounds, particularly in the low-energy IR spectral regions.[18] If $Pb_{1-x}Cd_xTe$ alloys are to be used to produce optoelectronic devices, the dispersion of their n- and k-values has to be known accurately across a wide spectral range. In this work, we investigated the optical properties of $Pb_{1-x}Cd_xTe$ alloys ($0 \leq x \leq 0.20$) using SE. X-ray measurements performed on $Pb_{1-x}Cd_xTe$ films indicated that they form rock-salt structures. In addition, these measurements show that their lattice parameters decrease as the Cd concentration is increased in

the alloy system. Using SE measurements, we determined the dispersion of the n and k values from 0.1 eV to 4.1 eV for each of the $Pb_{1-x}Cd_xTe$ alloys. Determining the *n* and *k* values of $Pb_{1-x}Cd_xTe$ alloys for the first time in the IR region is a significant contribution of this work. Additionally, upon further analysis of the n and k dispersion in $Pb_{1-x}Cd_xTe$ alloys, we found that their band gap increases as a function of the Cd concentration.

Experimental Details

Films of PbTe and $Pb_{1-x}Cd_xTe$ were deposited using the electron beam (e-beam) deposition onto 4" (100) Si wafers (MTI). The wafers were chemically degreased in methanol and acetone and treated in the UV-ozone cleaner. A dip in the dilute hydrofluoric acid (2%) was performed prior to deposition to remove the native silicon dioxide layer.

Polycrystalline PbTe (99.999%, Alfa Aesar) and $Pb_{1-x}Cd_xTe$ of three nominal compositions (x = 0.05, 0.10, and 0.15) were used as the source material. Polycrystalline $Pb_{1-x}Cd_xTe$ source material was synthesized using the vertical Bridgman method. Pre-weighed mixtures of PbTe and CdTe binary materials (99.999%, Alfa Aesar) were loaded in a sealed ampoule which was passed slowly through a two-zone furnace. The upper zone of the furnace was kept above the melting point of the compound and the lower zone was maintained below the melting point. Thus, the feed material in the ampoule melted in the upper zone and crystallized out as the ampoule entered the lower zone. This solidification process was gradual and started from the tip of the ampoule, with the melt-solid interface shifting upward (along the length of the ampoule) as it was dropped.

Film thicknesses and composition were confirmed using the Scanning Electron Microscopy (SEM) imaging and Energy Dispersive Spectroscopy (EDS) analysis. SEM-EDS measurements were performed on cleaved samples in a Hitachi S-4800 Cold-Field-Emission SEM equipped with an Oxford EDS system. The samples were imaged at an operating voltage of 3.0 kV while the EDS analysis was completed at an accelerating voltage of 20 kV. There were some deviations between the target and measured cadmium content (x) of the $Pb_{1-x}Cd_xTe$ films. These can be due to the segregation during the source material synthesis and/or preferential evaporation during the e-beam deposition. The target and measured cadmium content of $Pb_{1-x}Cd_xTe$ films, as well as film thicknesses measured using SEM, are given in Table 1.

Table 1: Composition and thicknesses of $Pb_{1-x}Cd_xTe$ Films

Sample #	Target Cadmium Content	Measured Cadmium Content	Film Thickness
	x	x	μm
A	0.05	0.02	1.03 – 1.05
B	0.10	0.06	1.07 – 1.09
C	0.15	0.20	1.03 – 1.04

Grazing incidence X-ray diffraction (GIXRD) patterns were collected using a Malvern Panalytical Empyrean® instrument fitted with a copper long-fine-focus X-ray tube operated at 45 kV and 40 mA. The incident beam path included a parallel beam X-ray mirror and a 0.5° divergence slit fixed at an incident angle of 1°. The diffracted beam path incorporated dCore® optics with a 0.28° parallel plate collimator and a PIXcel3D® detector operating in open detector (0D) mode with an active length of 14.025 mm. Spectroscopic ellipsometry measurements were

performed at incident angles of 65°, 70° and 75° using two Woollam ellipsometers (VASE and IR-VASE) that had a combined spectral range from far infrared (IR) to ultraviolet (i.e., 0.1 eV to 4.5 eV).

Results

The crystal structures of PbTe and CdTe are rock-salt and zinc-blende, respectively. According to theoretical calculations, $Pb_{1-x}Cd_xTe$ with rock-salt structure are stable only when Cd content is below 20% ($x < 0.2$).[17] Indeed, studies of $Pb_{1-x}Cd_xTe$ bulk crystals with $x \sim 0.2$, show that the alloy segregates into Pb and Cd rich phases.[9] Thus, there is a possibility of formation of CdTe inclusions in a rock-salt matrix for higher *x*-value samples. XRD measurements show formation of phase-pure rock-salt alloy, as shown in Fig 1(a). All peaks can be labeled as originating from rock-salt PbTe. In addition, with the increase in CdTe content, diffraction peaks steadily shift to larger angles. This indicates a decrease in the lattice constant with the increase in CdTe content. Calculated lattice parameters of $Pb_{1-x}Cd_xTe$ films are plotted as a function of CdTe content in Fig. 1(b). As expected, the lattice parameters decrease with the increase in CdTe content. The decrease is consistent – although somewhat smaller – than previously measured for bulk $Pb_{1-x}Cd_xTe$ crystals.[19]

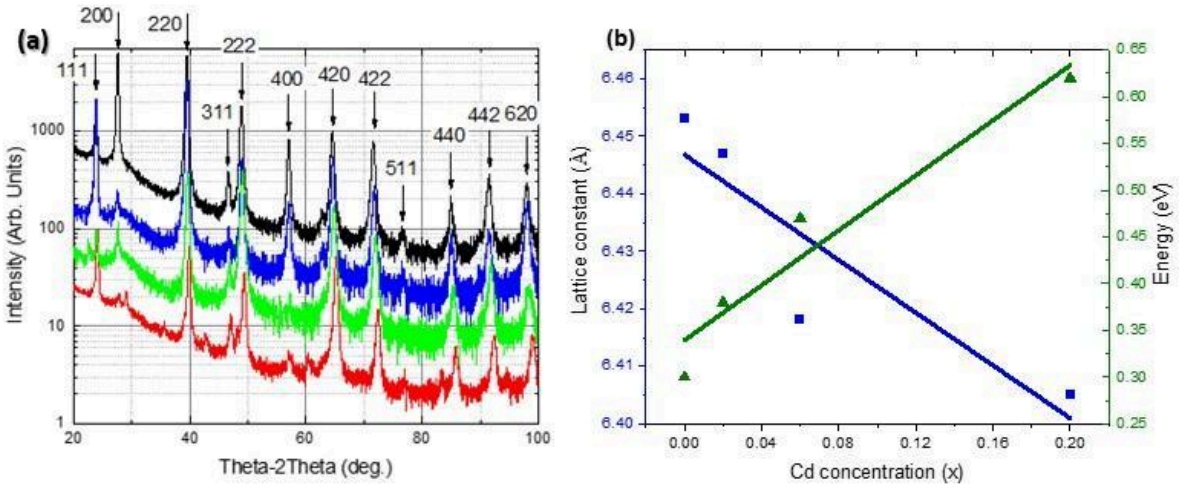

Figure 1. (a) X-ray diffraction patterns collected from PbTe (black), $Pb_{0.98}Cd_{0.02}Te$ (blue), $Pb_{0.94}Cd_{0.06}Te$ (green), and $Pb_{0.80}Cd_{0.20}Te$ (red) films. (b) Lattice constant and the bandgap energies of $Pb_{1-x}Cd_xTe$ films plotted as a function of Cd concentration. Solid symbols correspond to experimental data while the solid lines are linear fits.

We performed spectroscopic ellipsometry measurements on each of the $Pb_{1-x}Cd_xTe$ films to obtain their n and k. Ellipsometry measures two standard parameters, Ψ and Δ, at each wavelength of the spectrum, which are related to the ratio of the complex reflection coefficient for light polarized parallel to the plane of incidence and the complex reflection coefficient for light polarized perpendicular to the plane of incidence.[12] If a sample is made of several layers, both the *n* and *k* as well as the thicknesses of each layer affects the ellipsometry spectra.[13] Since ellipsometry is an inverse problem, one establishes a model to represent the sample structure, which consists of a sequence of layers with abrupt interfaces, bound by a semi-infinite substrate and the ambient. In our case, we used a three-layer model

to simulate the data which consisted of the Si substrate, $Pb_{1-x}Cd_xTe$ film and a rough-layer. While the optical constants of Si were obtained from published data,[20] the *n, k* and the thicknesses of the $Pb_{1-x}Cd_xTe$ film and a rough-layer were allowed to vary. The rough-layer was modeled using a Bruggemann effective medium approximation.[21] We then varied the model parameters and performed a regression analysis until the calculated and experimental data match with each other. In Fig. 2 and Fig. 3, we show the experimental (symbols) and model (solid line) data obtained for PbTe and $Pb_{0.80}Cd_{0.20}Te$, respectively. Similar data and fits were obtained for the other two $Pb_{1-x}Cd_xTe$ films. For all samples, we obtained spectroscopic scans at three angles of incidence (i.e., 65º, 70º and 75º) using two spectroscopic ellipsometers. Both Ψ and Δ in the IR region show maxima and minima which are due to thin film interference (see figures 2a, 2c, 3a and 3c). These features in the Ψ and Δ spectra are useful to determine the thicknesses of the $Pb_{1-x}Cd_xTe$ film and the rough-layer. The thicknesses we obtained for each film is shown in Table 2. The absence of the maxima and minima in Ψ and Δ spectra above ~1 eV signals the absorption of the film, as depicted in figures 2b, 2d, 3b and 3d. To optimize the fits, we had to incorporate a rough-layer on top of the $Pb_{1-x}Cd_xTe$ film. The thicknesses of the rough-layer are also shown in Table 2.

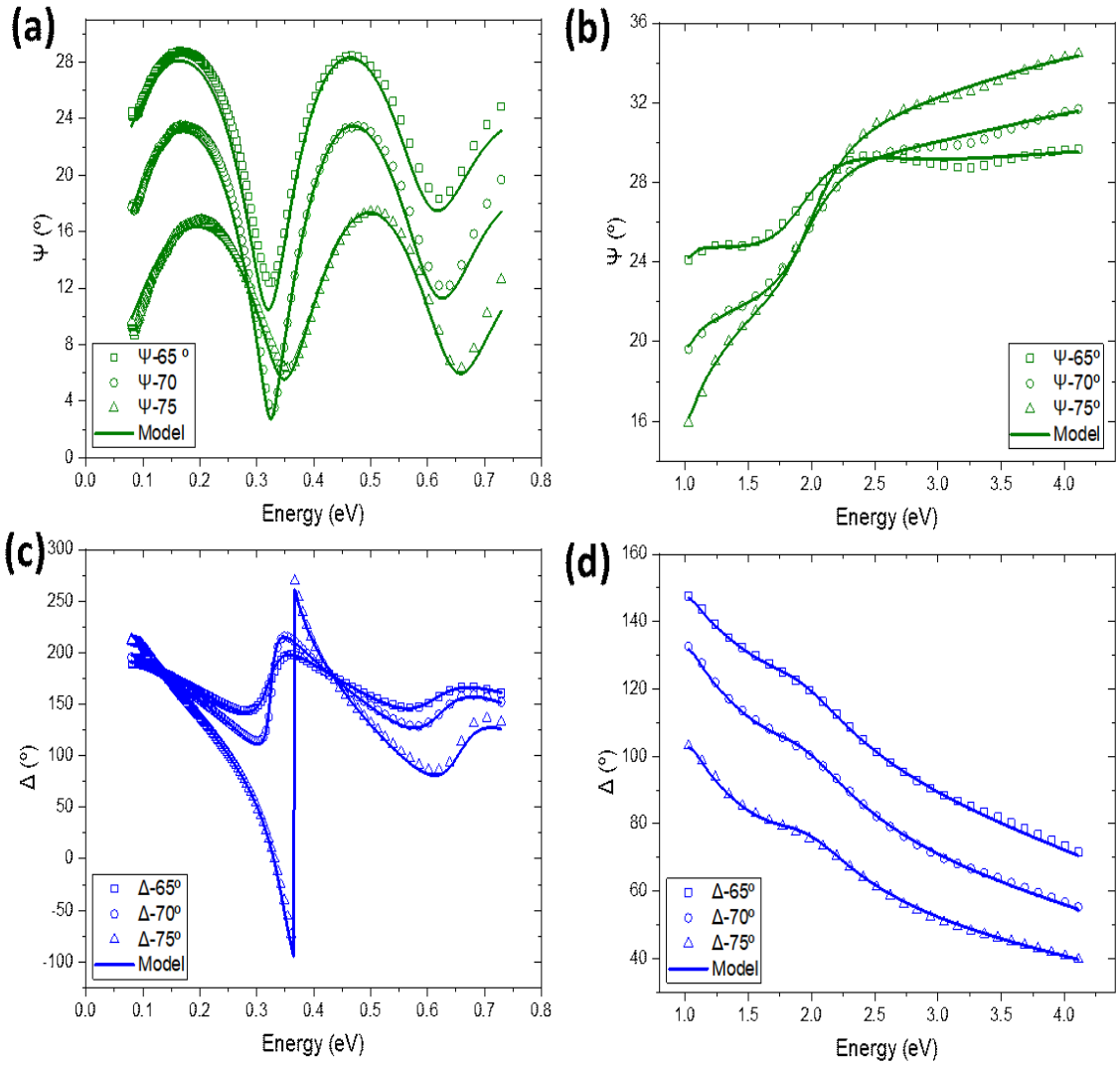

Figure 2. The experimental (symbols) and modeled (solid lines) spectra of PbTe obtained by the two ellipsometers. (a) and (b) show the Ψ spectra for the two spectral regions while (c) and (d) show the Δ spectra for the two regions.

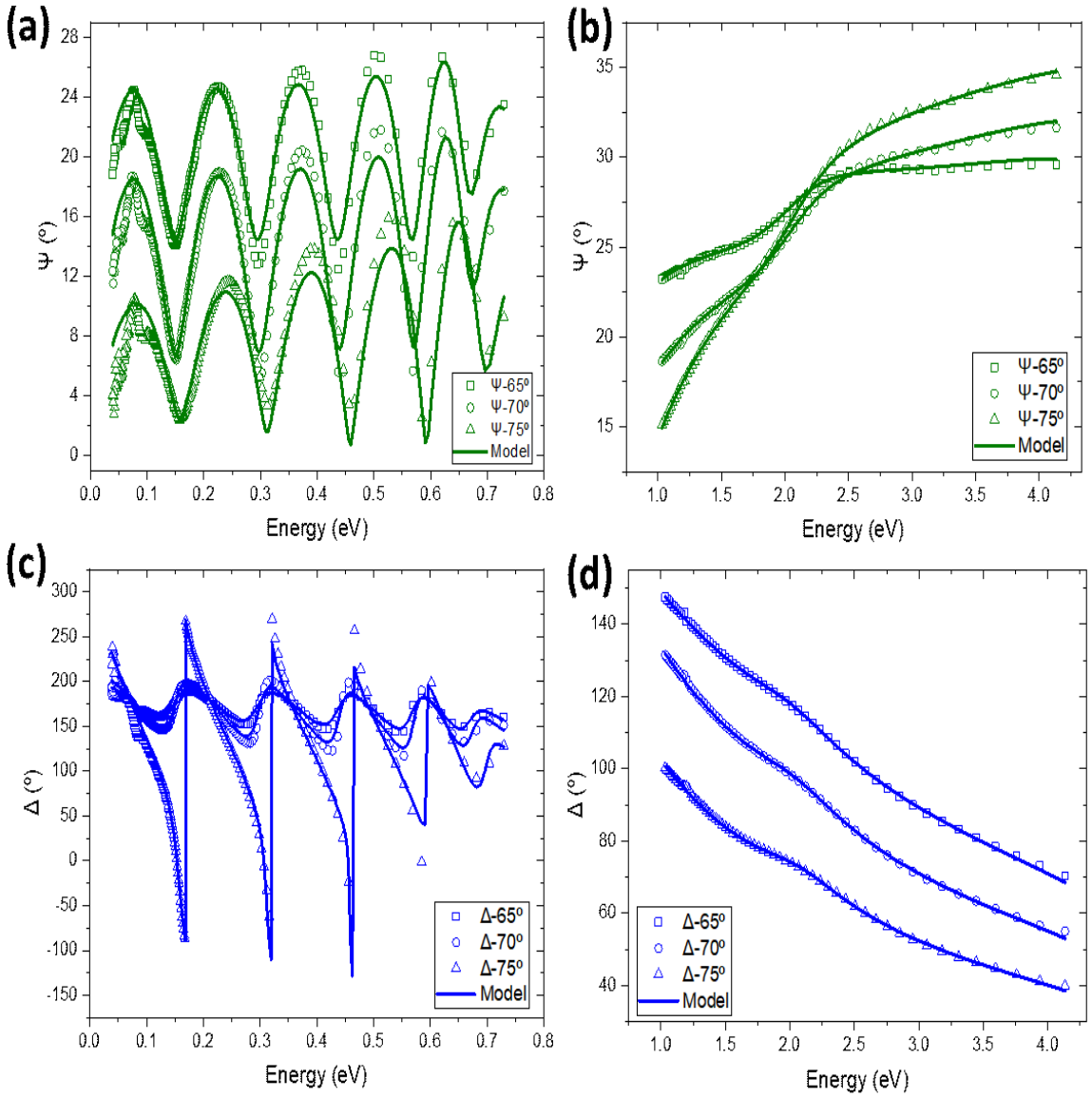

Figure 3. The experimental (symbols) and modeled (solid lines) spectra of $Pb_{0.80}Cd_{0.20}Te$ obtained by the two ellipsometers. (a) and (b) show the Ψ spectra for the two spectral regions while (c) and (d) show the Δ spectra for the two regions.

In order to determine *n* and *k* of each $Pb_{1-x}Cd_xTe$ film, we modeled the optical constants as a collections of Kramers-Kronig consistent oscillators, whose amplitude, energy-position and broadening parameters were adjusted to obtain a fit for the experimental data.[13] For the IR data, we used a single a Tauc-Lorentz oscillator to fit the Ψ and Δ spectra.[22] In this case, the oscillator-position corresponded to the fundamental band gap of $Pb_{1-x}Cd_xTe$, which are shown in Table 2 and also Fig. 1b. While SE is able to determine the phonon energies by analyzing the low-energy IR spectra,[23–25] these energies occur below our spectral region for the $Pb_{1-x}Cd_xTe$ alloys studied in this work.[26] In fitting the spectra above 1 eV, we included three Gaussian oscillators to obtain a good-fit to the experimental data. Initially, we fit the two spectral regions separately with their associate oscillators. Finally, we fit the entire spectral region simultaneously in order to obtain reliable dispersion models for $Pb_{1-x}Cd_xTe$ films. In Table 3, we show the parameters of the four oscillators used to fit the Ψ and Δ spectra for each $Pb_{1-x}Cd_xTe$ films.

Table 2. The lattice parameters determined from X-ray diffraction, the band gap and the thicknesses determined from spectroscopic ellipsometry are shown for all four $Pb_{1-x}Cd_xTe$ samples.

Sample	Lattice Parameter (Å)	Energy gap (eV)	Film thickness (nm)	Rough-layer thickness (nm)
PbTe	6.453	0.30	410 ± 20	20 ± 5
$Pb_{0.98}Cd_{0.02}Te$	6.447	0.38	950 ± 10	40 ± 10

$Pb_{0.94}Cd_{0.06}Te$	6.418	0.47	960 ± 10	30 ± 5
$Pb_{0.80}Cd_{0.20}Te$	6.405	0.62	1020 ± 10	20 ± 5

After realizing the energy gaps for $Pb_{1-x}Cd_xTe$ samples, one has to reconcile with the fact that Ψ and Δ spectra contain interference ripples above the band gap, as shown in figures 2a, 2c, 3a and 3c. After all, one would expect the light to be absorbed above the band gap energy, preventing it from transmitting and the reflecting back from the film-substrate interface to promote interference. The fact that one observes interference ripples above the band gap means that such waves are transmitted and reflected back to from interference ripples. This happens because the penetration depth ($=\lambda/4\pi k$, where k is the extinction coefficient) is reasonably close to the thickness of the film. For example, the penetration depth for PbTe at around 0.6 eV is ~500nm, which is larger than its thickness (410nm). Similar calculations indicate that the penetration depths of other alloys are also close to their film thicknesses, which then accounts for the interference ripples observed above their energy gaps. It is important to note that around 1 eV, the penetration depth for PbTe and $Pb_{1-x}Cd_xTe$ (x=0.80) are ~100nm and ~90nm, respectively. Since these values are much smaller than their film thicknesses, there is no opportunity for waves to travel to the film-substrate interface and reflect back to the surface to provide interference effects. This is the reason why there are no

interference ripples in the 1.0-4.1eV spectral range. In other words, the samples are much more absorbing in this energy range.

The *n* and *k* values obtained from our oscillator fits are shown in Fig. 4. Figures 4a and 4b show the dispersion of *n* while figures 4c and 4d show the dispersion of *k* determined for the two spectral regions of the ellipsometers. In the low-energy region shown in figures 4a and 4c, for most energies, the *n* and *k* values reduce as the concentration of Cd is increased in the $Pb_{1-x}Cd_xTe$ alloy system. The onset of absorption, exhibited by the non-zero dispersion of *k* in Fig. 4c, clearly indicates a blue-shift of the transition as the Cd concentration is increased. In the high-energy region shown in figures 4b and 4d, except for the $Pb_{0.80}Cd_{0.20}Te$ sample, the other alloys of $Pb_{1-x}Cd_xTe$ show a similar trend as observed for the low-energy region; both *n* and *k* values tend to reduce with the increase of Cd concentration. Interestingly, the *n* and *k* values of the $Pb_{0.80}Cd_{0.20}Te$ sample are more close to the values of the PbTe sample. Because of the difficulty involved in preparing alloys with higher concentration of Cd concentration, the ellipsometry beam may be exposing a region of sample that is slightly phase separated. While the SE that obtained the low-energy spectra (figures 4a and 4c) had a large input beam diameter of around 1 cm, the SE that obtained the high-energy spectra (figures 4b and 4d) had an input beam diameter of around 300 μm. Hence the low-energy spectra are averaged over a wide-sample region while the high-energy spectra are obtained for a much smaller region of the sample.

Table 3. The parameters of the four oscillators used to fit the ellipsometry spectra for all four $Pb_{1-x}Cd_xTe$ samples. Each oscillator is characterized by its amplitude (A), energy-position at its maximum amplitude (E_n) and broadening (Br) parameters. The Tauc-Lorentz oscillator has an additional parameter that specifies the onset of absorption (E_g).[22]

Sample	Tauc-Lorentz	Gauss-1	Gauss-2	Guass-3
PbTe	A=33.5 eV E_g=0.306 eV E_n=1.50 eV Br=11.4 eV	A=24.3 eV E_n=1.81 eV Br=0.94 eV	A=6.79 eV E_n=2.62 eV Br=1.93 eV	A=2.79 eV E_n=6.12 eV Br=4.87 eV
$Pb_{0.98}Cd_{0.02}Te$	A=47.0 eV E_g=0.383 eV E_n=1.54 eV Br=10.0 eV	A=11.1 eV E_n=1.15 eV Br=0.62 eV	A=4.85 eV E_n=1.65 eV Br=0.51 eV	A=3.66 eV E_n=1.98 eV Br=0.56 eV
$Pb_{0.94}Cd_{0.06}Te$	A=32.2 eV E_g=0.466 eV E_n=0.47 eV Br=8.0 eV	A=4.62 eV E_n=0.72 eV Br=0.84 eV	A=2.02 eV E_n=1.47 eV Br=1.2 eV	A=0.62 eV E_n=2.47 eV Br=3.53 eV
$Pb_{0.80}Cd_{0.20}Te$	A=125.4 eV E_g=0.620 eV E_n=0.62 eV Br=7.5 eV	A=14.9 eV E_n=1.89 eV Br=1.12 eV	A=3.84 eV E_n=2.91 eV Br=5.02 eV	A=1.90 eV E_n=5.02 eV Br=2.98 eV

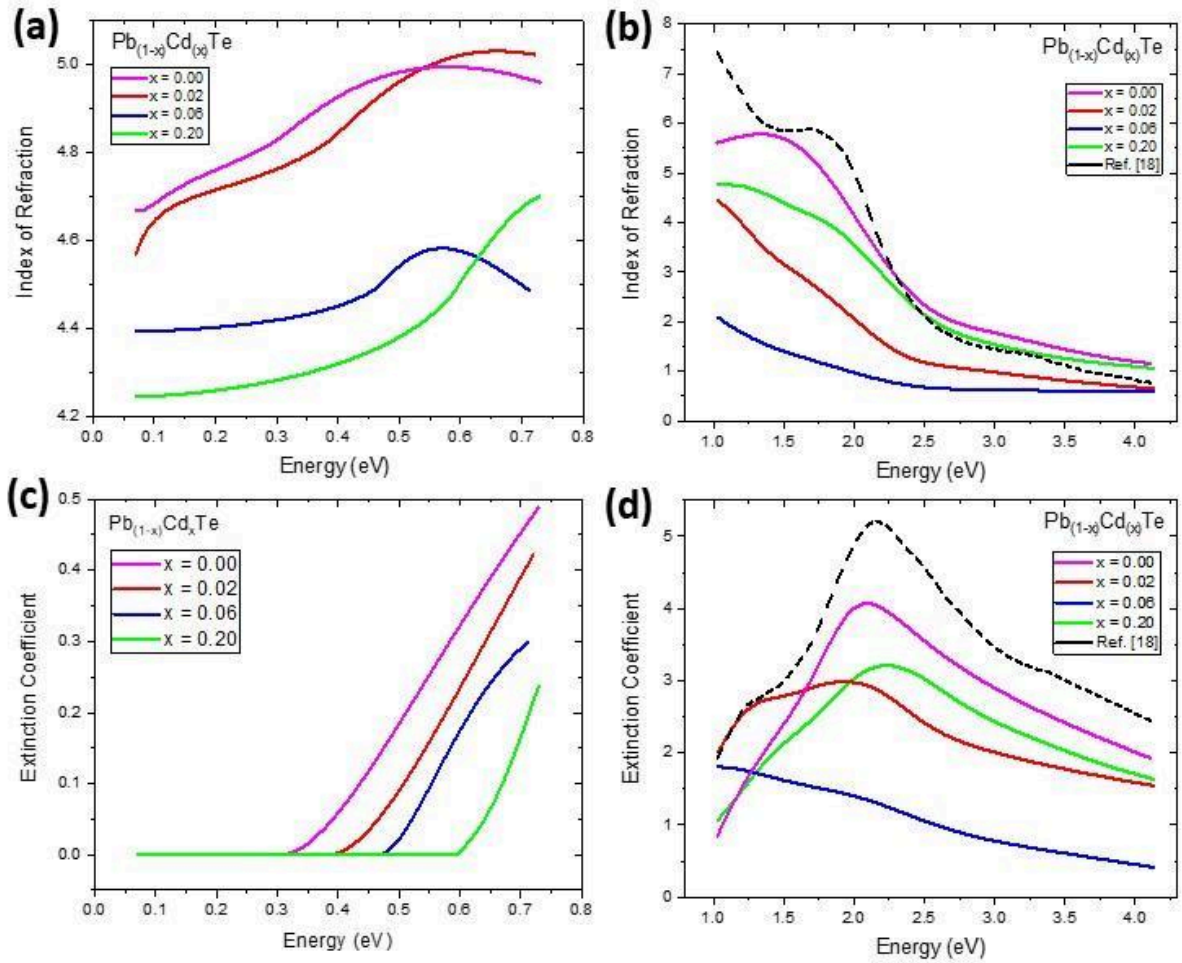

Figure 4. (a), (b) The index of refraction and (c), (d) the extinction coefficient obtained from ellipsometry measurements for the $Pb_{1-x}Cd_xTe$ films. The data shown in black in (b) and (d) are taken from Ref. 18.

It is instructive to focus on the *n* and *k* values obtained for PbTe. Density functional theory-calculations show that the valence band maximum and the conduction band minimum occur at the L-point in the Brillouin zone, which results in a direct band gap.[16,17,27,28] In general, SE detects the critical points of the band structure, which occur at points in the Brillouin zone where the joint density of states maximizes.[29] Besides the critical point

associated with the fundamental band gap at the L-point, previous studies have found three additional critical points for PbTe between 1 eV and 6 eV, occurring at 1.08 eV, 2.02 eV and 3.25 eV. (Ref. 18) Our analysis shows only two critical points at 1.8 eV and 2.6 eV in this region. This is possibly due to the fact that we included the oscillator describing the fundamental band gap (i.e., at 0.3 eV) in fitting our high-energy spectral range. Since the contribution of this oscillator extends into the ~1 eV range, our fit to the experimental spectra does not require an additional oscillator at ~1 eV, as was the case in previously published results. For PbTe, we note that the two additional critical points are associated with the transitions near the **Δ** and ***Σ*** points in the Brillouin zone.[17, 18] We also found two additional critical points in fitting the spectra of the other three films. These critical points did not show a particular trend as a function of Cd concentration.

Conclusion

In this study, we have determined the index of refraction and the extinction coefficient of four $Pb_{1-x}Cd_xTe$ ($0 \leq x \leq 0.20$) films between 0.1 eV and 4.1 eV. The lattice parameters of $Pb_{1-x}Cd_xTe$ films, grown using an e-beam deposition, complied with Vegard's law behavior, where their values decreased linearly as a function of Cd concentration. Modeling the spectroscopic ellipsometry spectra, the thicknesses and the optical constants were determined for each sample. In general, both the index of refraction and the extinction coefficient decreases across the entire spectrum as the Cd concentration increases. The film with the highest concentration of Cd (i.e., $Pb_{0.80}Cd_{0.20}Te$) slightly defies this trend, possibly due to some phase separation in the film. We further analyzed the optical functions, representing

them as a sum of oscillators that depict the electronic transitions associated with the Brillouin zone. The oscillator-position associated with the fundamental band gap blue-shifts as the Cd concentration is increased in the $Pb_{1-x}Cd_xTe$ films. For all four films, we also found two additional critical points that are associated with higher-order electronic transitions in the $Pb_{1-x}Cd_xTe$ alloy system.

Acknowledgments

The work at Kenyon was funded by the National Science Foundation (DMR-1909245). The work performed at RMD was supported by the Air Force SBIR, Contract # FA9451-22-P-A005. The views expressed are those of the author and do not necessarily reflect the official policy or position of the Department of the Air Force, the Department of Defense, or the U.S. government.

Distribution Statement: A-Approved for Public Release. Release # AFRL-2024-2240.

References

(1) Khiar, A.; Volobuev, V.; Witzan, M.; Hochreiner, A.; Eibelhuber, M.; Springholz, G. In-Well Pumped Mid-Infrared PbTe/CdTe Quantum Well Vertical External Cavity Surface Emitting Lasers. *Appl. Phys. Lett.* **2014**, *104* (23), 231105. https://doi.org/10.1063/1.4882081.

(2) Zogg, H.; Rahim, M.; Khiar, A.; Fill, M.; Felder, F.; Quack, N. Mid Infrared Resonant Cavity Detectors and Lasers with Epitaxial Lead-Chalcogenides. *Opto-Electron. Rev.* **2010**, *18* (3), 231–235. https://doi.org/10.2478/s11772-010-1028-5.

(3) Hochreiner, A.; Schwarzl, T.; Eibelhuber, M.; Heiss, W.; Springholz, G.; Kolkovsky, V.; Karczewski, G.; Wojtowicz, T. Midinfrared Electroluminescence from PbTe/CdTe Quantum Dot Light-Emitting Diodes. *Appl. Phys. Lett.* **2011**, *98* (2), 021106. https://doi.org/10.1063/1.3531760.

(4) Heremans, J. P.; Jovovic, V.; Toberer, E. S.; Saramat, A.; Kurosaki, K.; Charoenphakdee, A.; Yamanaka, S.; Snyder, G. J. Enhancement of Thermoelectric Efficiency in PbTe by Distortion of the Electronic Density of States. *Science* **2008**, *321* (5888), 554–557. https://doi.org/10.1126/science.1159725.

(5) Biswas, K.; He, J.; Blum, I. D.; Wu, C.-I.; Hogan, T. P.; Seidman, D. N.; Dravid, V. P.; Kanatzidis, M. G. High-Performance Bulk Thermoelectrics with All-Scale Hierarchical Architectures. *Nature* **2012**, *489* (7416), 414–418. https://doi.org/10.1038/nature11439.

(6) Zhang, Q.; Wang, H.; Zhang, Q.; Liu, W.; Yu, B.; Wang, H.; Wang, D.; Ni, G.; Chen, G.; Ren, Z. Effect of Silicon and Sodium on Thermoelectric Properties of Thallium-Doped Lead Telluride-Based Materials. *Nano Lett.* **2012**, *12* (5), 2324–2330. https://doi.org/10.1021/nl3002183.

(7) Zhang, B.; Lu, P.; Liu, H.; Jiao, L.; Ye, Z.; Jaime, M.; Balakirev, F. F.; Yuan, H.; Wu, H.; Pan, W.; Zhang, Y. Quantum Oscillations in a Two-Dimensional Electron Gas at the Rocksalt/Zincblende Interface of PbTe/CdTe (111) Heterostructures. *Nano Lett.* **2015**, *15* (7), 4381–4386. https://doi.org/10.1021/acs.nanolett.5b01605.

(8) Buczko, R.; Cywiński, Ł. PbTe/PbSnTe Heterostructures as Analogs of Topological Insulators. *Phys. Rev. B* **2012**, *85* (20), 205319. https://doi.org/10.1103/PhysRevB.85.205319.

(9) Scheidt, T.; Rohwer, E. G.; Von Bergmann, H. M.; Saucedo, E.; Diéguez, E.; Fornaro, L.; Stafast, H. Optical Second-Harmonic Imaging of PbxCd1−xTe Ternary Alloys. *J. Appl. Phys.* **2005**, *97* (10), 103104. https://doi.org/10.1063/1.1899224.

(10) Yuan, S.; Krenn, H.; Springholz, G.; Ueta, Y.; Bauer, G.; McCann, P. J. Magnetoreflectivity of PbEuTe Epilayers and PbTe/PbEuTe Multiple Quantum Wells. *Phys. Rev. B* **1997**, *55* (7), 4607–4619. https://doi.org/10.1103/PhysRevB.55.4607.

(11) Adachi, S.; Kimura, T.; Suzuki, N. Optical Properties of CdTe: Experiment and Modeling. *J. Appl. Phys.* **1993**, *74* (5), 3435–3441. https://doi.org/10.1063/1.354543.

(12) R.M.A. Azzam, N.M. Bashara. *Ellipsometry and Polarized Light,*; North Holland Publishing Company, Amsterdam-New York-Oxford., 1977.

(13) Fujiwara, H. *Spectroscopic Ellipsometry: Principles and Applications*; John Wiley & Sons, 2007.

(14) Dinh, D. V.; Peiris, F.; Lähnemann, J.; Brandt, O. Optical Properties of ScN Layers Grown on Al2O3(0001) by Plasma-Assisted Molecular Beam Epitaxy. *Appl. Phys. Lett.* **2023**, *123* (11), 112102. https://doi.org/10.1063/5.0164058.

(15) Romero, A. H.; Cardona, M.; Kremer, R. K.; Lauck, R.; Siegle, G.; Serrano, J.; Gonze, X. C. Lattice Properties of PbX (X=S, Se, Te): Experimental Studies and Ab Initio Calculations Including Spin-Orbit Effects. *Phys. Rev. B* **2008**, *78* (22), 224302. https://doi.org/10.1103/PhysRevB.78.224302.

(16) Ye, Z.; Cui, S.; Shu, T.; Ma, S.; Liu, Y.; Sun, Z.; Luo, J.-W.; Wu, H. Electronic Band

Structure of Epitaxial PbTe (111) Thin Films Observed by Angle-Resolved Photoemission Spectroscopy. *Phys. Rev. B* **2017**, *95* (16), 165203. https://doi.org/10.1103/PhysRevB.95.165203.
(17) Bukała, M.; Sankowski, P.; Buczko, R.; Kacman, P. Structural and Electronic Properties of Pb 1 − x Cd x Te and Pb 1 − x Mn x Te Ternary Alloys. *Phys. Rev. B* **2012**, *86* (8), 085205. https://doi.org/10.1103/PhysRevB.86.085205.
(18) Norihiro Suzuki; Adachi, S. Optical Properties of PbTe. *Jpn. J. Appl. Phys.* **1994**, *33* (193). https://doi.org/10.1143/JJAP.33.193.
(19) Szot, M.; Szczerbakow, A.; Dybko, K.; Kowalczyk, L.; Smajek, E.; Domukhovski, V.; Łusakowska, E.; Dziawa, P.; Mycielski, A.; Story, T.; Bukała, M.; Galicka, M.; Sankowski, P.; Buczko, R.; Kacman, P. Experimental and Theoretical Analysis Of PbTe-CdTe Solid Solution Grown by Physical Vapour Transport Method. *Acta Phys. Pol. A* **2009**, *116* (5), 959–961. https://doi.org/10.12693/APhysPolA.116.959.
(20) Aspnes, D. E.; Studna, A. A. Dielectric Functions and Optical Parameters of Si, Ge, GaP, GaAs, GaSb, InP, InAs, and InSb from 1.5 to 6.0 eV. *Phys. Rev. B* **1983**, *27* (2), 985–1009. https://doi.org/10.1103/PhysRevB.27.985.
(21) Aspnes, D. E.; Theeten, J. B.; Hottier, F. Investigation of Effective-Medium Models of Microscopic Surface Roughness by Spectroscopic Ellipsometry. *Phys. Rev. B* **1979**, *20* (8), 3292–3302. https://doi.org/10.1103/PhysRevB.20.3292.
(22) Jellison, G. E., Jr.; Modine, F. A. Parameterization of the Optical Functions of Amorphous Materials in the Interband Region. *Appl. Phys. Lett.* **1996**, *69* (3), 371–373. https://doi.org/10.1063/1.118064.
(23) Schubert, M.; Tiwald, T. E.; Herzinger, C. M. Infrared Dielectric Anisotropy and Phonon Modes of Sapphire. *Phys. Rev. B* **2000**, *61* (12), 8187–8201. https://doi.org/10.1103/PhysRevB.61.8187.
(24) Mandal, N.; Peiris, F. C.; Maksimov, O.; Tamargo, M. C. Far-Infrared Dielectric Functions and Phonon Spectra of BexZn1−xTe Alloys Determined by Spectroscopic Ellipsometry. *Solid State Commun.* **2009**, *149* (39), 1698–1701. https://doi.org/10.1016/j.ssc.2009.06.016.
(25) Lyons, J. W.; Brill, G.; Peiris, F. C. Far-Infrared Optical Properties of Hg1−xCdxSe Thin Films. *Solid State Commun.* **2019**, *303–304*, 113729. https://doi.org/10.1016/j.ssc.2019.113729.
(26) Wu, H.; Cao, C.; Si, J.; Xu, T.; Zhang, H.; Wu, H.; Chen, J.; Shen, W.; Dai, N. Observation of Phonon Modes in Epitaxial PbTe Films Grown by Molecular Beam Epitaxy. *J. Appl. Phys.* **2007**, *101* (10), 103505. https://doi.org/10.1063/1.2714682.
(27) Tung, Y. W.; Cohen, M. L. Relativistic Band Structure and Electronic Properties of SnTe, GeTe, and PbTe. *Phys. Rev.* **1969**, *180* (3), 823–826. https://doi.org/10.1103/PhysRev.180.823.
(28) Rogers, L. M.; Crocker, A. J. Transport Properties of the CdxPb1−x Te Alloy System. *J. Phys. Appl. Phys.* **1971**, *4* (7), 1006. https://doi.org/10.1088/0022-3727/4/7/318.
(29) P.Y. Yu, M. Cardona. *Fundamentals of Semiconductors*; Springer: Berlin, 1996.